PHYSICAL REVIEW B **91**, 144108 (2015)

Atomic resolution imaging using electron energy-loss phonon spectroscopy

N. R. Lugg,[1] B. D. Forbes,[2] S. D. Findlay,[3] and L. J. Allen[2,*]

[1]*Institute of Engineering Innovation, School of Engineering, University of Tokyo, Tokyo 113-8656, Japan*

[2]*School of Physics, University of Melbourne, Parkville, Victoria 3010, Australia*

[3]*School of Physics and Astronomy, Monash University, Clayton, Victoria 3800, Australia*

(Received 11 February 2015; published 20 April 2015)

Recent developments have improved the attainable energy resolution in electron energy-loss spectroscopy in aberration-corrected scanning transmission electron microscopy to the order of 10 meV. In principle, this allows spectroscopy and imaging of crystals using the phonon sector of the energy-loss spectrum at atomic resolution, a supposition supported by recent simulations for molecules. Here we show that the "quantum excitation of phonons" model encapsulates the physics necessary to simulate the atomic resolution imaging of crystals based on phonon excitation and we explore the predictions of such simulations.

DOI: 10.1103/PhysRevB.91.144108 PACS number(s): 61.05.jd

I. INTRODUCTION

In scanning transmission electron microscopy (STEM), the widely used technique of high-angle annular dark-field (HAADF) imaging, also known as *Z*-contrast imaging, is based on detecting the number of electrons scattered into an annular detector as a function of the raster scan position of the incident probe. Since the inner angle of the HAADF detector is typically three to five times that of the probe-forming aperture, the flux of elastically scattered electrons reaching the detector is small compared with that of electrons which have been inelastically scattered to large angles after excitation (or deexcitation) of one or more phonons (also known as thermal diffuse scattering). Whereas the electron energy in the incident STEM probe is usually of the order of 100 keV, the energy losses (gains) from phonon excitation (deexcitation) are typically of the order of tens of meV. The trend from ionization and plasmon scattering events suggests that low energy losses correspond to delocalized interactions, but even given the very low energy losses involved, phonon-scattering interactions are localized enough to routinely allow atomic resolution HAADF STEM images. An interesting question is whether the electrons thermally scattered through smaller angles also undergo interactions with sufficient localization for atomic resolution imaging. Recent theoretical simulations for molecules predict that in practice atomic resolution imaging of crystals should be possible [1,2] without the high-angle selection offered by HAADF imaging. Recent experimental work on strontium titanate explored this [3]. Such images may extend characterization techniques by allowing the mapping of light elements such as hydrogen and lithium [4], for which phonon excitations may be more localized and also have a stronger signal than core-loss ionization signals.

Electrons thermally scattered through the range of angles up to roughly twice that of the probe forming aperture in STEM are in a region of the diffraction plane where elastic scattering usually dominates and, in the absence of energy selection, there is usually no way to separate out the contribution from thermally scattered electrons—although this is possible using electron holography [5]. However, given a monochromated electron beam and an energy-loss spectrometer with sufficient energy resolution one can directly monitor the change in the phonon subsector of the energy-loss spectrum as a function of probe position for electrons scattered through smaller angles. The quest for better energy resolution in electron energy-loss spectroscopy in STEM has recently seen a resolution as fine as 10 meV achieved [6]. Using a system with a significantly coarser energy resolution, Egoavil *et al.* [3] explored atomic resolution imaging for electrons thermally scattered into a series of on-axis disk detectors with increasing outer angle. The smallest outer angle was 38 mrad, less than twice the probe-forming aperture of 21 mrad, and the largest was 225 mrad. Isolating the phonon sector of the energy-loss spectrum involves a delicate removal of the zero-loss peak which, as they pointed out, has been done in an indirect manner, complicating the interpretation of the images obtained, which nevertheless exhibit atomic-scale features.

Here we explore what would be obtained if direct subtraction of the zero-loss peak from the spectra could be performed. The calculations are based on the quantum excitation of phonons (QEP) model due to Forbes *et al.* [7]. We note that in some previous work this model was referred to as the Born-Oppenheimer model, due to an approximation used in its derivation. This model is based on rigorous many-body quantum mechanics and, as we shall establish here by several arguments, accounts for all phonon excitations occurring in the target as well as the associated energy losses. Furthermore, this model has the advantage that the intensity due to thermal scattering can be separated from the intensity due to elastic scattering. The QEP model sits within the framework of nonrelativistic quantum scattering theory, in which inelastic scattering, such as that which occurs via phonon excitation, is accounted for as quantum excitations of the scattering target, thus allowing for the calculation of atomic resolution images based on phonon excitation.

The paper is structured as follows. In Sec. II we present some key steps in the derivation of the QEP model with an emphasis on those showing that all final states of the target after phonon excitation are taken into account. In Sec. III we illustrate this by examining the simple case of scattering from a single atom, treated as a quantum harmonic oscillator using two approaches: first, the thermally scattered intensity is calculated by summing the intensity contributions due to

*lja@unimelb.edu.au

transitions from an initial state of the system to all possible final states, using the transition potential formulation [8–10]; and second, we calculate the thermally scattered intensity within the QEP model and obtain the same result. In Sec. IV we demonstrate that thermal statistics of the initial target state can be accounted for. In Sec. V the energy losses associated with phonon excitation are more explicitly identified within the framework of the QEP model. In Sec. VI we present simulations of images based on the low-loss (phonon) part of the energy-loss spectrum.

II. THE QUANTUM EXCITATION OF PHONONS MODEL

In this section we rework the QEP model [7], with the intention of emphasizing that all final states of the system after excitation (or deexcitation) of a phonon are accounted for in the model.

A fundamental approach to modeling inelastic excitations based on many-body quantum mechanics is encapsulated in the coupled-channels formalism of Yoshioka [11]. In this approach, each inelastic wave function describing the fast electron after it has excited a phonon in the target is considered on an individual basis. In the QEP model, we are able to model the collective effect of all phonon interactions using only a single function. We explain this in more detail below.

The Hamiltonian of the total system comprised of fast electron and target can be decomposed as

$$H(\mathbf{r},\boldsymbol{\tau}_\mathrm{n},\boldsymbol{\tau}_\mathrm{e}) = T(\mathbf{r}) + H_\mathrm{c}(\boldsymbol{\tau}_\mathrm{n},\boldsymbol{\tau}_\mathrm{e}) + H'(\mathbf{r},\boldsymbol{\tau}_\mathrm{n},\boldsymbol{\tau}_\mathrm{e}), \quad (1)$$

where $\mathbf{r}$ is the coordinate of the incident electron, $\boldsymbol{\tau}_\mathrm{n}$ is shorthand for the set of all the coordinates $\boldsymbol{\tau}_\mathrm{n}^i$ of the nuclei in the target, and $\boldsymbol{\tau}_\mathrm{e}$ is the set of all the coordinates $\boldsymbol{\tau}_\mathrm{e}^i$ of the electrons in the target. The term $T(\mathbf{r})$ represents the kinetic energy of the fast electron, $H_\mathrm{c}(\boldsymbol{\tau}_\mathrm{n},\boldsymbol{\tau}_\mathrm{e})$ is the Hamiltonian for the target (often a crystal, hence the subscript c), and $H'(\mathbf{r},\boldsymbol{\tau}_\mathrm{n},\boldsymbol{\tau}_\mathrm{e})$ is the Hamiltonian describing the interaction between the fast electron and the target.

The many-body wave function for the system of incoming electron and target can be expanded in terms of the complete set of eigenstates ξ_m of the target Hamiltonian as [11]

$$\Psi(\mathbf{r},\boldsymbol{\tau}_\mathrm{n},\boldsymbol{\tau}_\mathrm{e}) = \sum_m \psi_m(\mathbf{r})\xi_m(\boldsymbol{\tau}_\mathrm{n},\boldsymbol{\tau}_\mathrm{e}). \quad (2)$$

The inelastic wave functions $\psi_m(\mathbf{r})$ ($m \neq 0$) describe the fast electron after a transition in which the target is left in the final state $\xi_m(\boldsymbol{\tau}_\mathrm{n},\boldsymbol{\tau}_\mathrm{e})$. The elastic wave function $\psi_0(\mathbf{r})$ describes the fast electron prior to scattering and also after leaving the target in the initial state $\xi_0(\boldsymbol{\tau}_\mathrm{n},\boldsymbol{\tau}_\mathrm{e})$. We note that $\xi_0(\boldsymbol{\tau}_\mathrm{n},\boldsymbol{\tau}_\mathrm{e})$ denotes an arbitrary initial state, not necessarily the ground state of the target.

We are interested primarily in phonon excitation and thus assume that the nuclear and electronic subsystems are decoupled and that the electronic subsystem is not excited. This is consistent with how target wave functions are treated in previous models of phonon excitation [12,13]. Therefore we make the factorization

$$\xi_m(\boldsymbol{\tau}_\mathrm{n},\boldsymbol{\tau}_\mathrm{e}) = a_m(\boldsymbol{\tau}_\mathrm{n})b(\boldsymbol{\tau}_\mathrm{e},\boldsymbol{\tau}_\mathrm{n}), \quad (3)$$

where $b(\boldsymbol{\tau}_\mathrm{e},\boldsymbol{\tau}_\mathrm{n})$ is the wave function describing the electrons in the target. It is assumed that each electron can be associated with a particular atom in the target and that the electronic coordinates $\boldsymbol{\tau}_\mathrm{e}$ are defined relative to the pertinent nuclear coordinates [12]. We note that the normalization of the electronic wave function $b(\boldsymbol{\tau}_\mathrm{e},\boldsymbol{\tau}_\mathrm{n})$ is independent of the nuclear coordinates $\boldsymbol{\tau}_\mathrm{n}$. The wave functions $a_m(\boldsymbol{\tau}_\mathrm{n})$ describe the state of the nuclear subsystem and can be constructed either as the product of harmonic oscillator wave functions for each *atom* (if independent atomic vibrations are assumed [12]) or as the product of harmonic oscillator wave functions for each *vibrational mode* (if correlated atomic motion is modeled [13]).

Substituting Eq. (3) into Eq. (2) yields the following expression for the many-body wave function:

$$\Psi(\mathbf{r},\boldsymbol{\tau}_\mathrm{n},\boldsymbol{\tau}_\mathrm{e}) = b(\boldsymbol{\tau}_\mathrm{e},\boldsymbol{\tau}_\mathrm{n})\sum_m \psi_m(\mathbf{r})a_m(\boldsymbol{\tau}_\mathrm{n}). \quad (4)$$

We note, due to the boundary conditions imposed, that when the incident electron is far from the target we have

$$\Psi(\mathbf{r},\boldsymbol{\tau}_\mathrm{n},\boldsymbol{\tau}_\mathrm{e}) \to a_0(\boldsymbol{\tau}_\mathrm{n})b(\boldsymbol{\tau}_\mathrm{e},\boldsymbol{\tau}_\mathrm{n})\psi_0(\mathbf{r}). \quad (5)$$

Consistent with these boundary conditions, we factor out the initial state of the nuclear subsystem $a_0(\boldsymbol{\tau}_\mathrm{n})$ in Eq. (4) to obtain

$$\Psi(\mathbf{r},\boldsymbol{\tau}_\mathrm{n},\boldsymbol{\tau}_\mathrm{e}) = a_0(\boldsymbol{\tau}_\mathrm{n})b(\boldsymbol{\tau}_\mathrm{e},\boldsymbol{\tau}_\mathrm{n})\sum_m \psi_m(\mathbf{r})\frac{a_m(\boldsymbol{\tau}_\mathrm{n})}{a_0(\boldsymbol{\tau}_\mathrm{n})}. \quad (6)$$

Let us now define

$$\phi(\mathbf{r},\boldsymbol{\tau}_\mathrm{n}) \equiv \sum_m \psi_m(\mathbf{r})\frac{a_m(\boldsymbol{\tau}_\mathrm{n})}{a_0(\boldsymbol{\tau}_\mathrm{n})}, \quad (7)$$

so that we can write the wave function of the system as

$$\Psi(\mathbf{r},\boldsymbol{\tau}_\mathrm{n},\boldsymbol{\tau}_\mathrm{e}) = a_0(\boldsymbol{\tau}_\mathrm{n})b(\boldsymbol{\tau}_\mathrm{e},\boldsymbol{\tau}_\mathrm{n})\phi(\mathbf{r},\boldsymbol{\tau}_\mathrm{n}). \quad (8)$$

If we can calculate the quantity $\phi(\mathbf{r},\boldsymbol{\tau}_\mathrm{n})$ then we can construct the wave function for the system $\Psi(\mathbf{r},\boldsymbol{\tau}_\mathrm{n},\boldsymbol{\tau}_\mathrm{e})$. This provides an alternative approach for calculating $\Psi(\mathbf{r},\boldsymbol{\tau}_\mathrm{n},\boldsymbol{\tau}_\mathrm{e})$ to that of explicitly obtaining all the functions $\psi_m(\mathbf{r})$ and $a_m(\boldsymbol{\tau}_\mathrm{n})$ in Eq. (4), which is what one must do in the coupled-channels formalism.

The form for the wave function of the system given in Eq. (8) can be substituted into the many-body Schrödinger equation and the appropriate boundary conditions applied. The details are given in Appendix A. The following governing equations for the functions $\phi(\mathbf{r},\boldsymbol{\tau}_\mathrm{n})$ and $a_0(\boldsymbol{\tau}_\mathrm{n})$ are then obtained:

$$\left[-\frac{\hbar^2}{2m_\mathrm{e}}\nabla_\mathbf{r}^2 + \widetilde{H}'(\mathbf{r},\boldsymbol{\tau}_\mathrm{n}) - \sum_j \frac{\hbar^2}{2M_j}\left\{\nabla_{\boldsymbol{\tau}_\mathrm{n}^j}^2 + \frac{2}{a_0(\boldsymbol{\tau}_\mathrm{n})}\nabla_{\boldsymbol{\tau}_\mathrm{n}^j}a_0(\boldsymbol{\tau}_\mathrm{n})\cdot\nabla_{\boldsymbol{\tau}_\mathrm{n}^j}\right\}\right]\phi(\mathbf{r},\boldsymbol{\tau}_\mathrm{n}) = E_0\phi(\mathbf{r},\boldsymbol{\tau}_\mathrm{n}), \quad (9)$$

$$-\sum_i \frac{\hbar^2}{2M_j}\nabla_{\boldsymbol{\tau}_\mathrm{n}^j}^2 a_0(\boldsymbol{\tau}_\mathrm{n}) + \widetilde{H}'_\mathrm{c}(\boldsymbol{\tau}_\mathrm{n})a_0(\boldsymbol{\tau}_\mathrm{n}) = \epsilon_0^{(\mathrm{n})}a_0(\boldsymbol{\tau}_\mathrm{n}). \quad (10)$$

In Eq. (9) $\widetilde{H}'(\mathbf{r},\boldsymbol{\tau}_\mathrm{n})$ is the interaction Hamiltonian integrated over the electronic degrees of freedom $\boldsymbol{\tau}_\mathrm{e}$, E_0 is the energy of the incoming electron, $\hbar$ is the reduced Planck's constant,

and m_e is the electron mass. We denote by M_j the mass of the jth nucleus. In Eq. (10) $\widetilde{H}'_c(\boldsymbol{\tau}_n)$ is the target Hamiltonian integrated up over the electronic degrees of freedom and $\epsilon_0^{(n)}$ is the energy associated with the initial state of the target nuclear subsystem. We note that while it may appear that any function of $\boldsymbol{\tau}_n$ could have been factored out of the sum in Eq. (6), $a_0(\boldsymbol{\tau}_n)$ is in fact a choice that satisfies Eq. (10) *exactly*.

In Eq. (9) the terms on the middle line depend on gradients of $\phi(\mathbf{r},\boldsymbol{\tau}_n)$ with respect to $\boldsymbol{\tau}_n$ and the inverse of the nuclear masses. As changes in $\phi(\mathbf{r},\boldsymbol{\tau}_n)$ with respect to either $\mathbf{r}$ or $\boldsymbol{\tau}_n$ occur over approximately the same length scale, it is reasonable to assume that acting on $\phi(\mathbf{r},\boldsymbol{\tau}_n)$ with either the $\mathbf{r}$ or $\boldsymbol{\tau}_n$ gradient operator will result in functions of approximately the same order of magnitude. However, as the nuclear masses M_j are many orders of magnitude greater than the electron mass m_e, these terms will not make a significant contribution to the energy associated with the function $\phi(\mathbf{r},\boldsymbol{\tau}_n)$. Therefore, in what follows we will drop these terms. This approximation is in the spirit of the Born-Oppenheimer approximation used in molecular physics [14].

In previous work [7] the assumption was made that $\phi(\mathbf{r},\boldsymbol{\tau}_n)$ satisfies

$$\nabla_{\boldsymbol{\tau}_n^j}\phi(\mathbf{r},\boldsymbol{\tau}_n)\approx\mathbf{0}, \tag{11}$$

an assumption that is not strictly necessary. Rather, it is only necessary that the quantity in the curly brackets in Eq. (9) be not large, so that when multiplied by the prefactor $1/M_j$ the terms remain small.

Dropping those terms on the middle line in Eq. (9) yields the following approximate governing equation for $\phi(\mathbf{r},\boldsymbol{\tau}_n)$:

$$-\frac{\hbar^2}{2m_e}\nabla_{\mathbf{r}}^2\phi(\mathbf{r},\boldsymbol{\tau}_n)+\widetilde{H}'(\mathbf{r},\boldsymbol{\tau}_n)\phi(\mathbf{r},\boldsymbol{\tau}_n)=E_0\phi(\mathbf{r},\boldsymbol{\tau}_n). \tag{12}$$

Equation (12), with the real-valued potential $\widetilde{H}'(\mathbf{r},\boldsymbol{\tau}_n)$, has the form of a Schrödinger equation for elastic scattering from a target with parametrically fixed $\boldsymbol{\tau}_n$ and can be solved using the multislice approach. We note however that despite having the *form* of an elastic scattering equation, the complete space of solutions $\phi(\mathbf{r},\boldsymbol{\tau}_n)$ does in fact encode all details of inelastic scattering via phonon excitation. The parametric dependence on the nuclear coordinates $\boldsymbol{\tau}_n$ provides an extra degree of freedom, from which the inelastically scattered states can be explicitly retrieved. This is shown in detail below. We note furthermore that the potential $\widetilde{H}'(\mathbf{r},\boldsymbol{\tau}_n)$ in Eq. (12) is not what would normally be used for calculations of elastic scattering. Rather, one would use the potential

$$H_{00}(\mathbf{r})=\int|\xi_0(\boldsymbol{\tau}_n,\boldsymbol{\tau}_e)|^2H'(\mathbf{r},\boldsymbol{\tau}_n,\boldsymbol{\tau}_e)\,d\boldsymbol{\tau}_n\,d\boldsymbol{\tau}_e, \tag{13}$$

the interaction potential averaged with respect to the initial state of the target. As such, solutions obtained using this potential represent purely elastic scattering. In contrast, the extra degrees of freedom (i.e., the nuclear coordinates $\boldsymbol{\tau}_n$) in the potential $\widetilde{H}'(\mathbf{r},\boldsymbol{\tau}_n)$, which is expressed explicitly as

$$\widetilde{H}'(\mathbf{r},\boldsymbol{\tau}_n)=\int|b(\boldsymbol{\tau}_e)|^2H'(\mathbf{r},\boldsymbol{\tau}_n,\boldsymbol{\tau}_e)\,d\boldsymbol{\tau}_e, \tag{14}$$

expand the solution space to account for inelastic scattering.

We emphasize that, as can be seen from Eq. (7), the functions $\phi(\mathbf{r},\boldsymbol{\tau}_n)$ contain information on the excited states of the nuclear subsystem and all transitions to phonon-excited states of the target are implicitly contained in the wave function of the form in Eq. (8). Invoking orthogonality of the eigenstates $a_m(\boldsymbol{\tau}_n)$ we can write

$$\psi_m(\mathbf{r})=\int a_m^*(\boldsymbol{\tau}_n)a_0(\boldsymbol{\tau}_n)\phi(\mathbf{r},\boldsymbol{\tau}_n)\,d\boldsymbol{\tau}_n, \tag{15}$$

which shows that functions $\psi_m(\mathbf{r})$ describing the fast electron after (phonon) excitation of the target to the state $a_m(\boldsymbol{\tau}_n)$ can be retrieved from the right-hand side of Eq. (7).

The intensity distribution of the fast electron is modeled by the quantum-mechanical average over the coordinates of particles in the target:

$$\begin{aligned}I(\mathbf{r})&=\int|\Psi(\mathbf{r},\boldsymbol{\tau}_n,\boldsymbol{\tau}_e)|^2\,d\boldsymbol{\tau}_n\,d\boldsymbol{\tau}_e\\&=\int|a_0(\boldsymbol{\tau}_n)|^2|\phi(\mathbf{r},\boldsymbol{\tau}_n)|^2\,d\boldsymbol{\tau}_n.\end{aligned} \tag{16}$$

For the purposes of efficient calculation, this integral can be treated as a Monte Carlo calculation, with $|a_0(\boldsymbol{\tau}_n)|^2$ assuming the role of a probability distribution from which nuclear configurations $\boldsymbol{\tau}_n$ are drawn at random. From Eq. (15) the wave function for those electrons which have been elastically scattered is

$$\psi_0(\mathbf{r})=\int|a_0(\boldsymbol{\tau}_n)|^2\phi(\mathbf{r},\boldsymbol{\tau}_n)\,d\boldsymbol{\tau}_n \tag{17}$$

and the corresponding intensity is

$$I_{el}(\mathbf{r})=\left|\int|a_0(\boldsymbol{\tau}_n)|^2\phi(\mathbf{r},\boldsymbol{\tau}_n)\,d\boldsymbol{\tau}_n\right|^2. \tag{18}$$

A comparison of Eqs. (16) and (18) shows that there is more electron density in the total scattered intensity than there is in the elastic channel, because the former sums the intensities of the functions $\phi(\mathbf{r},\boldsymbol{\tau}_n)$ while the latter sums the same functions coherently, leading to phase interference which reduces the resulting intensity. Any disparity between the total and elastic electron densities therefore comes from the inelastic (phonon excitation) channels. Consequently we are able to decompose the scattered intensity into contributions from elastically scattered and thermally scattered electrons (those that have excited a phonon, perhaps multiple times). The intensity corresponding to electrons which have been thermally scattered is given by

$$\begin{aligned}I_{th}(\mathbf{r})&=I(\mathbf{r})-I_{el}(\mathbf{r})\\&=\int|a_0(\boldsymbol{\tau}_n)|^2|\phi(\mathbf{r},\boldsymbol{\tau}_n)|^2\,d\boldsymbol{\tau}_n\\&\quad-\left|\int|a_0(\boldsymbol{\tau}_n)|^2\phi(\mathbf{r},\boldsymbol{\tau}_n)\,d\boldsymbol{\tau}_n\right|^2.\end{aligned} \tag{19}$$

We reiterate that despite Eq. (19) above having no explicit reference to the final states of the target (after phonon excitation), those final states are in fact represented in the thermally scattered intensity calculated in this manner. This has been made clear by the theoretical formulation above [see

in particular Eq. (7)]. In the next section, we demonstrate this explicitly for a simplified model.

III. THERMAL SCATTERING FROM A SINGLE OSCILLATING ATOM

In this section we demonstrate explicitly that the theoretical framework developed in the previous section accounts for phonon excitation. We restrict our attention to the case of a fast electron scattering from a single atom sitting in an isotropic harmonic potential, an approach which permits an explicit, analytical calculation of various quantities. In a similar manner to how vibrations are treated in the Einstein model of solids, we can consider the harmonic potential to be an effective external potential due to the rest of the charged particles in the system, a reasonable approximation for an atom sitting in a crystal. We begin with a calculation of the functions describing the fast electron after excitation of the target to each final state, which is done explicitly within the transition potential formulation. These are used to construct the thermally scattered intensity. We then construct this quantity within the framework of the QEP model and arrive at the same result.

A. Transition potential formulation

Within the transition potential formulation, the functions $\psi_m(\mathbf{r})$ [see Eq. (2)] can be calculated as [8–10]

$$\psi_m(\mathbf{r}_\perp) = -i\sigma H_{m0}(\mathbf{r}_\perp)\psi_0(\mathbf{r}_\perp, z_m), \tag{20}$$

where $\mathbf{r}_\perp$ is the transverse component of the fast electron coordinate $\mathbf{r}$, $\sigma = m_e\lambda/2\pi\hbar^2$ is the interaction strength, λ is the de Broglie wavelength of the fast electron, $\psi_0(\mathbf{r}_\perp, z_m)$ is the wave function corresponding to elastic scattering of the fast electron, and z_m is the point along the optical axis at which the inelastic event m occurs. The projected transition potential $H_{m0}(\mathbf{r}_\perp)$ is given by

$$H_{m0}(\mathbf{r}_\perp) = \int H_{m0}(\mathbf{r}) e^{-2\pi i(k_m - k_0)z}\, dz, \tag{21}$$

where $H_{m0}(\mathbf{r})$ is the transition potential defined by

$$H_{m0}(\mathbf{r}) = \int \xi_m^*(\boldsymbol{\tau}_n, \boldsymbol{\tau}_e) H'(\mathbf{r}, \boldsymbol{\tau}_n, \boldsymbol{\tau}_e) \xi_0(\boldsymbol{\tau}_n, \boldsymbol{\tau}_e)\, d\boldsymbol{\tau}_n\, d\boldsymbol{\tau}_e, \tag{22}$$

and k_0 and k_m are the wave numbers associated with the electron before and after inelastic scattering. The functions $\xi_0(\boldsymbol{\tau}_n, \boldsymbol{\tau}_e)$ and $\xi_m(\boldsymbol{\tau}_n, \boldsymbol{\tau}_e)$ are the initial and final states of the harmonic oscillator.

We show in Appendix B that the transition potentials can be given in reciprocal space as

$$H_{m0}(\mathbf{q}) = -e f_e(\mathbf{q}) \int a_m^*(\boldsymbol{\tau}_n) a_0(\boldsymbol{\tau}_n) e^{-2\pi i \mathbf{q}\cdot\boldsymbol{\tau}_n}\, d\boldsymbol{\tau}_n, \tag{23}$$

where e is the absolute value of the electron charge and $f_e(\mathbf{q})$ is the electron scattering factor defined as

$$f_e(\mathbf{q}) \equiv \int V(\mathbf{r}) e^{-2\pi i \mathbf{q}\cdot\mathbf{r}}\, d\mathbf{r}, \tag{24}$$

with $V(\mathbf{r})$ the Coulomb potential of the atom.

Equation (20) can be rewritten in reciprocal space as

$$\begin{aligned}\psi_m(\mathbf{q}_\perp) &= -i\sigma H_{m0}(\mathbf{q}_\perp) \otimes \psi_0(\mathbf{q}_\perp) \\ &= i\sigma e \left[f_e(\mathbf{q}_\perp) \int a_m^*(\boldsymbol{\tau}_n) a_0(\boldsymbol{\tau}_n) e^{-2\pi i \mathbf{q}_\perp\cdot\boldsymbol{\tau}_n}\, d\boldsymbol{\tau}_n \right] \\ &\quad \otimes \psi_0(\mathbf{q}_\perp),\end{aligned} \tag{25}$$

where $\mathbf{q}_\perp$ is the transverse wave vector and $\otimes$ denotes the convolution operator. The z_m dependence has now been dropped since the scattering potential is that of a single atom at a single z position.

The thermally scattered intensity in the diffraction plane is given by

$$I_{th}(\mathbf{q}_\perp) = \sum_{m\neq 0} |\psi_m(\mathbf{q}_\perp)|^2. \tag{26}$$

Restricting our attention for now to the case of plane wave illumination, for which $\psi_0(\mathbf{q}_\perp) = \delta(\mathbf{q}_\perp)$, we have

$$\begin{aligned}I_{th}(\mathbf{q}_\perp) = \sigma^2 e^2 f_e^2(\mathbf{q}_\perp) \sum_{m\neq 0} &\int a_m^*(\boldsymbol{\tau}_n) a_0(\boldsymbol{\tau}_n) e^{-2\pi i \mathbf{q}_\perp\cdot\boldsymbol{\tau}_n}\, d\boldsymbol{\tau}_n \\ &\times \int a_m(\boldsymbol{\tau}_n') a_0^*(\boldsymbol{\tau}_n') e^{2\pi i \mathbf{q}_\perp\cdot\boldsymbol{\tau}_n'}\, d\boldsymbol{\tau}_n'.\end{aligned} \tag{27}$$

The functions $a_m(\boldsymbol{\tau}_n)$ are harmonic oscillator wave functions and obey the completeness identity $\sum_m a_m^*(\boldsymbol{\tau}_n) a_m(\boldsymbol{\tau}_n') = \delta(\boldsymbol{\tau}_n - \boldsymbol{\tau}_n')$. We can thus simplify the above to

$$I_{th}(\mathbf{q}_\perp) = \sigma^2 e^2 f_e^2(\mathbf{q}_\perp) \left[1 - \left| \int |a_0(\boldsymbol{\tau}_n)|^2 e^{-2\pi i \mathbf{q}_\perp\cdot\boldsymbol{\tau}_n}\, d\boldsymbol{\tau}_n \right|^2 \right]. \tag{28}$$

We note that explicitly summing over the final states leads to an expression depending only on the initial state.

The case of general illumination is treated in Appendix C.

B. QEP model

We now proceed to calculate the thermally scattered intensity within the QEP model, according to Eq. (19). Consistent with the approximations made within the transition potential formulation, the solution to Eq. (12) for $\phi(\mathbf{r}, \boldsymbol{\tau}_n)$ is found within the weak phase object approximation. The scattered portion is given by

$$\phi(\mathbf{r}_\perp, \boldsymbol{\tau}_n) = -i\sigma \widetilde{H}'_{proj}(\mathbf{r}_\perp, \boldsymbol{\tau}_n) \phi_0(\mathbf{r}_\perp). \tag{29}$$

Here $\widetilde{H}'_{proj}(\mathbf{r}_\perp, \boldsymbol{\tau}_n)$ is the z projection of $\widetilde{H}'(\mathbf{r}, \boldsymbol{\tau}_n)$, where the latter is the interaction potential $H'(\mathbf{r}, \boldsymbol{\tau}_n, \boldsymbol{\tau}_e)$ with electronic degrees of freedom integrated out. The projected potential $\widetilde{H}'_{proj}(\mathbf{r}_\perp, \boldsymbol{\tau}_n)$ can be identified as $-eV_{proj}(\mathbf{r}_\perp - \boldsymbol{\tau}_n)$ where $V_{proj}(\mathbf{r}_\perp)$ is the z projection of the Coulomb potential of the atom. The function $\phi_0(\mathbf{r}_\perp)$ is the boundary condition on Eq. (12) and can be identified with $\psi_0(\mathbf{r}_\perp)$, the illumination at the entrance surface. We note the similarity in form between Eq. (29) and Eq. (20). We thus have

$$\phi(\mathbf{r}_\perp, \boldsymbol{\tau}_n) = i\sigma e V_{proj}(\mathbf{r}_\perp - \boldsymbol{\tau}_n) \psi_0(\mathbf{r}_\perp), \tag{30}$$

and in reciprocal space this can be expressed as

$$\phi(\mathbf{q}_\perp, \boldsymbol{\tau}_n) = i\sigma e [f_e(\mathbf{q}_\perp) e^{-2\pi i \mathbf{q}_\perp\cdot\boldsymbol{\tau}_n}] \otimes \psi_0(\mathbf{q}_\perp), \tag{31}$$

where the phase factor $e^{-2\pi i \mathbf{q}_\perp \cdot \boldsymbol{\tau}_n}$ shifts the atomic potential to the position $\boldsymbol{\tau}_n$ and where $f_e(\mathbf{q}_\perp)$ is a slice at $q_z = 0$ of the electron scattering factor defined in Eq. (24).

For plane wave illumination, we have

$$\phi(\mathbf{q}_\perp, \boldsymbol{\tau}_n) = i\sigma e f_e(\mathbf{q}_\perp) e^{-2\pi i \mathbf{q}_\perp \cdot \boldsymbol{\tau}_n}, \tag{32}$$

and the thermally scattered intensity is thus given by [see Eq. (19)]

$$\begin{aligned} I_{\text{th}}(\mathbf{q}_\perp) &= \int |a_0(\boldsymbol{\tau}_n)|^2 |\phi(\mathbf{q}_\perp, \boldsymbol{\tau}_n)|^2 \, d\boldsymbol{\tau}_n \\ &\quad - \left| \int |a_0(\boldsymbol{\tau}_n)|^2 \phi(\mathbf{q}_\perp, \boldsymbol{\tau}_n) \, d\boldsymbol{\tau}_n \right|^2 \\ &= \sigma^2 e^2 f_e^2(\mathbf{q}_\perp) \int |a_0(\boldsymbol{\tau}_n)|^2 \, d\boldsymbol{\tau}_n \\ &\quad - \left| \sigma e f_e(\mathbf{q}_\perp) \int |a_0(\boldsymbol{\tau}_n)|^2 e^{-2\pi i \mathbf{q}_\perp \cdot \boldsymbol{\tau}_n} \, d\boldsymbol{\tau}_n \right|^2 \\ &= \sigma^2 e^2 f_e^2(\mathbf{q}_\perp) \left[1 - \left| \int |a_0(\boldsymbol{\tau}_n)|^2 e^{-2\pi i \mathbf{q}_\perp \cdot \boldsymbol{\tau}_n} \, d\boldsymbol{\tau}_n \right|^2 \right]. \end{aligned} \tag{33}$$

This result is identical to that obtained within the transition potential formulation [see Eq. (28)].

The case of general illumination is treated in Appendix C.

IV. STATISTICS OF INITIAL STATES

It is important to note that the agreement obtained for the thermally scattered intensity in the previous section between the transition potential formulation (in which final states are explicitly summed) and the QEP model (in which they are not) is not restricted to the ground state of the oscillating atom—the initial state $a_0(\boldsymbol{\tau}_n)$ can refer to an arbitrary initial state.

In practice, each electron contributing to an electron micrograph has scattered from a different initial state of the specimen, and those states are drawn from a thermal statistical ensemble. We will show in this section that, for the harmonic oscillator model, the thermal average can be easily accounted for, and is consistent with treating atomic displacements as Gaussian random deviates using mean-squared displacements measured experimentally.

Let us consider for the moment the total intensity scattered according to the QEP model:

$$I(\mathbf{r}) = \int |a_0(\boldsymbol{\tau}_n)|^2 |\phi(\mathbf{r}, \boldsymbol{\tau}_n)|^2 \, d\boldsymbol{\tau}_n. \tag{34}$$

Assuming the atomic motion in the target is that of independent, isotropic harmonic oscillators, the initial state of the target $a_0(\boldsymbol{\tau}_n)$ can be written as a product of 1D harmonic oscillator states. Furthermore, if one makes the ground state approximation, then all of those states are the harmonic oscillator ground state, in which case we can write $a_0(\boldsymbol{\tau}_n)$ as

$$a_0(\boldsymbol{\tau}_n) = \prod_j \prod_i A_0(\tau_{j,i}), \tag{35}$$

where j indexes a specific nucleus, $i = x, y, z$ is a Cartesian coordinate, and

$$A_0(\tau) = \left(\frac{M\omega}{\pi\hbar} \right)^{1/4} e^{-M\omega\tau^2/2\hbar}. \tag{36}$$

The probability density function $|a_0(\boldsymbol{\tau}_n)|^2$ is given by [as a corollary of Eq. (35)]

$$|a_0(\boldsymbol{\tau}_n)|^2 = \prod_j \prod_i |A_0(\tau_{j,i})|^2. \tag{37}$$

We must however consider that the initial state of the target may not be the ground state. We thus allow $A_0(\tau)$ to be an arbitrary harmonic oscillator wave function

$$\begin{aligned} A_0(\tau) \to g_n(\tau) &= \frac{1}{\sqrt{2^n n!}} \left(\frac{M\omega}{\pi\hbar} \right)^{1/4} \\ &\quad \times e^{-M\omega\tau^2/2\hbar} H_n\left(\sqrt{\frac{M\omega}{\hbar}} \tau \right), \end{aligned} \tag{38}$$

and furthermore, we allow for a statistical average of initial states, whereby the probability distribution $|A_0(\tau)|^2$ is given by

$$|A_0(\tau)|^2 \to \frac{1}{\mathcal{Z}} \sum_n e^{-E_n\beta} |g_n(\tau)|^2, \tag{39}$$

where $E_n = \hbar\omega(n + \frac{1}{2})$ is the energy of the nth thermal state, $\beta = 1/k_B T$, k_B is the Boltzmann constant, T is the temperature, and $\mathcal{Z}$ is the partition function, given by

$$\mathcal{Z} = \sum_n e^{-E_n\beta} = \frac{e^{-\hbar\omega\beta/2}}{1 - e^{-\hbar\omega\beta}}. \tag{40}$$

We show in Appendix D that Eq. (39) can now be rewritten as

$$|A_0(\tau)|^2 \to \frac{1}{\sqrt{2\pi\sigma^2}} e^{-\tau^2/2\sigma^2}, \tag{41}$$

where

$$\sigma^2 = \frac{\hbar}{2M\omega} \coth(\hbar\omega\beta/2). \tag{42}$$

The probability distribution $|a_0(\boldsymbol{\tau}_n)|^2$ for the displacements of the nuclei is given by the product of factors of the form in Eq. (41) for each nucleus and each direction, with M and ω specific to each nucleus. The quantity σ^2 can be shown to be the mean-squared displacement $\langle \tau^2 \rangle$ corresponding to the distribution $|A_0(\tau)|^2$. Experimentally measured Debye-Waller factors (which relate directly to the mean-squared displacement of an atom) can be utilized to determine the effective $|a_0(\boldsymbol{\tau}_n)|^2$ to be used in Eq. (34). We make the replacement $|a_0(\boldsymbol{\tau}_n)|^2 \to P(\boldsymbol{\tau}_n)$ to emphasize the fact that, in calculations, we use an *effective* probability distribution $P(\boldsymbol{\tau}_n)$ for the atomic displacements that includes the effects of thermal averaging, rather than referring explicitly to the target state $a_0(\boldsymbol{\tau}_n)$.

V. ENERGY LOSSES WITHIN THE QEP MODEL

Equation (12) is the governing equation for the auxiliary fast electron function $\phi(\mathbf{r}, \boldsymbol{\tau}_n)$. It has been shown formally (in general) and explicitly (specifically for the single harmonic

oscillator) that $\phi(\mathbf{r},\boldsymbol{\tau}_\mathrm{n})$ accounts for all the final states of the target. However, Eq. (12) contains on its right-hand side only the energy E_0, which is the energy of the incident electron. It is not immediately obvious where the energy losses are that should necessarily arise during excitation of the target system.

To illuminate the issue, we substitute Eq. (7) into Eq. (12),

$$\left[-\frac{\hbar^2}{2m_\mathrm{e}}\nabla_\mathbf{r}^2+\widetilde{H}'(\mathbf{r},\boldsymbol{\tau}_\mathrm{n})\right]\sum_m \psi_m(\mathbf{r})\frac{a_m(\boldsymbol{\tau}_\mathrm{n})}{a_0(\boldsymbol{\tau}_\mathrm{n})} = E_0\sum_m \psi_m(\mathbf{r})\frac{a_m(\boldsymbol{\tau}_\mathrm{n})}{a_0(\boldsymbol{\tau}_\mathrm{n})}, \tag{43}$$

and bring the operator inside the sum on the left-hand side,

$$\sum_m \left[E_m+\widetilde{H}'(\mathbf{r},\boldsymbol{\tau}_\mathrm{n})\right]\psi_m(\mathbf{r})\frac{a_m(\boldsymbol{\tau}_\mathrm{n})}{a_0(\boldsymbol{\tau}_\mathrm{n})} = E_0\sum_m \psi_m(\mathbf{r})\frac{a_m(\boldsymbol{\tau}_\mathrm{n})}{a_0(\boldsymbol{\tau}_\mathrm{n})}, \tag{44}$$

where E_m is the kinetic energy of the fast electron after having excited the target to state m. Rearranging this yields

$$\sum_m (E_0-E_m)\psi_m(\mathbf{r})\frac{a_m(\boldsymbol{\tau}_\mathrm{n})}{a_0(\boldsymbol{\tau}_\mathrm{n})} = \sum_m \widetilde{H}'(\mathbf{r},\boldsymbol{\tau}_\mathrm{n})\psi_m(\mathbf{r})\frac{a_m(\boldsymbol{\tau}_\mathrm{n})}{a_0(\boldsymbol{\tau}_\mathrm{n})}, \tag{45}$$

demonstrating that the energy losses E_0-E_m appear explicitly within the framework of the QEP model. These energy losses on the left-hand side of Eq. (45) are balanced on the right-hand side by the interaction potential energy between the target and fast electron in the mth excited state. Another perspective is that Eq. (12) is an implicit statement of conservation of energy, which can be restated in the form of Eq. (45) above in terms of the energy losses associated with each inelastic channel.

VI. SIMULATIONS

In Sec. III we dealt with the case of a single oscillating atom, for which an analytical solution could be found for the thermally scattered intensity in both the transition potential formulation and the QEP model. In this section we deal with the more relevant case of the scattering from a crystal. This is, in general, a nonlinear scattering problem for which an analytical solution cannot be found. However, a numerical solution can be obtained in a straightforward manner.

The thermally scattered intensity is obtained by using Eq. (19). We replace the initial target state probability distribution $|a_0(\boldsymbol{\tau}_\mathrm{n})|^2$ with a thermally averaged distribution $P(\boldsymbol{\tau}_\mathrm{n})$ (as discussed in Sec. IV). We furthermore include explicitly the dependence on the probe position $\mathbf{R}$ [which enters the calculation via the boundary conditions on the solution to Eq. (12)] and express the intensity as a function of the transverse wave vector $\mathbf{q}_\perp$ (as we are seeking to calculate intensities in the diffraction plane):

$$I_\mathrm{th}(\mathbf{q}_\perp,\mathbf{R}) = \int P(\boldsymbol{\tau}_\mathrm{n})|\phi(\mathbf{q}_\perp,\mathbf{R},\boldsymbol{\tau}_\mathrm{n})|^2\,d\boldsymbol{\tau}_\mathrm{n} - \left|\int P(\boldsymbol{\tau}_\mathrm{n})\phi(\mathbf{q}_\perp,\mathbf{R},\boldsymbol{\tau}_\mathrm{n})\,d\boldsymbol{\tau}_\mathrm{n}\right|^2. \tag{46}$$

Working within the Einstein model, the probability distribution $P(\boldsymbol{\tau}_\mathrm{n})$ decomposes into independent distributions for each atom, for which experimental values can be found in the literature for a particular specimen and temperature.

The function $\phi(\mathbf{r},\boldsymbol{\tau}_\mathrm{n})$ for any given nuclear configuration $\boldsymbol{\tau}_\mathrm{n}$ can be found by solving Eq. (12) using the multislice approach. The boundary conditions are provided by the known illumination. Furthermore, evaluation of the integrals in Eq. (46) can be performed using a Monte Carlo procedure, whereby values of $\boldsymbol{\tau}_\mathrm{n}$ at which to solve for $\phi(\mathbf{r},\boldsymbol{\tau}_\mathrm{n})$ are drawn at random from the distribution $P(\boldsymbol{\tau}_\mathrm{n})$ until convergence of the intensity is achieved.

In this section we will consider an imaging mode in which a convergent probe is scanned across the surface of a specimen while recording the flux of electrons entering an aperture in the diffraction plane. Furthermore we assume that only thermally scattered electrons (i.e., those which have excited a phonon) contribute to the signal. In this way, we calculate a two-dimensional image of the specimen based on thermal scattering.

For the present study we consider a specimen of ⟨100⟩ strontium titanate (STO) with a thickness ranging between 100 Å and 600 Å. An accelerating voltage of 120 kV is assumed. The convergence semiangle of the probe is 21 mrad and the probe-forming lens is assumed to be unaberrated. We use 30 nuclear configurations drawn at random from the appropriate distribution as part of the Monte Carlo procedure outlined above.

Figure 1 shows the probability density for the thermal component of the electron intensity in the diffraction plane as a function of scattering angle, with the probe placed above strontium, titanium/oxygen, and oxygen columns. The area under the graph between any two given scattering angles indicates the relative intensity that would be scattered into an annular detector spanning that range. These results were calculated for a specimen thickness of 200 Å. We note that in all three cases, thermal scattering is most likely to occur at scattering angles of around 50 mrad (roughly twice the semiangle of the probe-forming aperture), although it is

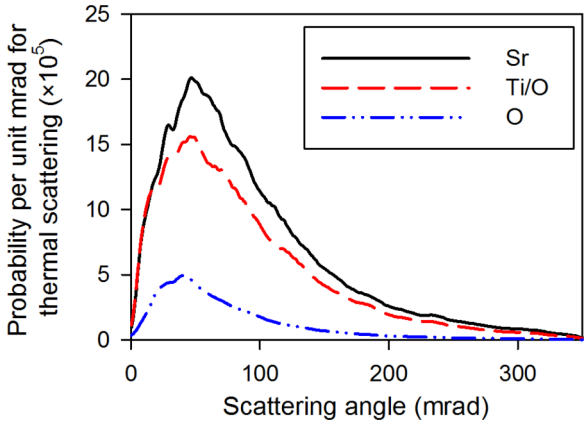

FIG. 1. (Color online) Probability density for the thermally scattered intensity in the diffraction plane as a function of scattering angle for an unaberrated convergent electron beam of accelerating voltage 120 kV and convergence semiangle 21 mrad incident upon a 200 Å thick specimen of ⟨100⟩ STO. The probe has been placed above strontium, titanium/oxygen, and oxygen columns.

distributed over a large range of scattering angles. High-angle annular dark field (HAADF) STEM images are formed by integrating the intensity scattered to large angles where thermal scattering dominates over elastic scattering. By examining the area under the graphs in Fig. 1, it is clear that the HAADF imaging mode does not count the significant contribution of those electrons that have been thermally scattered to lower angles. This is an unavoidable consequence of the fact that, in the absence of energy filtering, the low-angle scattering cannot be separated into elastic and thermal components. The inner angle of the HAADF detector is thus deliberately chosen to exclude elastically scattered electrons which would otherwise introduce deleterious coherence effects into the image formation. However, in the context of new capabilities in energy filtering (as discussed in the Introduction), it becomes interesting to investigate the potential of image formation using electrons thermally scattered to lower angles.

Figure 2 shows STEM images indicating the fraction of the incident electron flux which has been thermally scattered into the indicated range of angles as a function of probe position and for different specimen thicknesses, using the parameters specified above. These images correspond to what

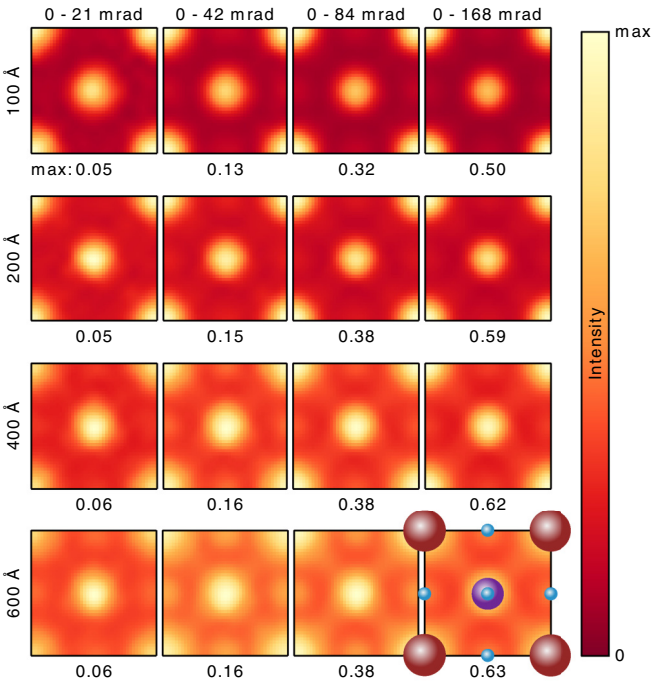

FIG. 2. (Color online) Maps of the fractional intensity of the thermal component of the intensity incident upon an aperture placed in the diffraction plane. We have assumed an unaberrated convergent electron beam of accelerating voltage 120 kV and convergence semiangle 21 mrad, incident upon a specimen of ⟨100⟩ STO. The maps are for four detectors spanning the angular ranges indicated and for four different specimen thicknesses. The calculations were performed using the QEP model, which accounts for phonon excitations in the target. Each image is displayed on an intensity scale ranging from zero to its individual maximum, which is noted below each panel. The specimen structure is overlaid in the bottom right panel. Large (brown) circles indicate columns of strontium atoms, medium (brown) circles indicate the presence of titanium atoms in a column, and small (blue) circles indicate the presence of oxygen atoms.

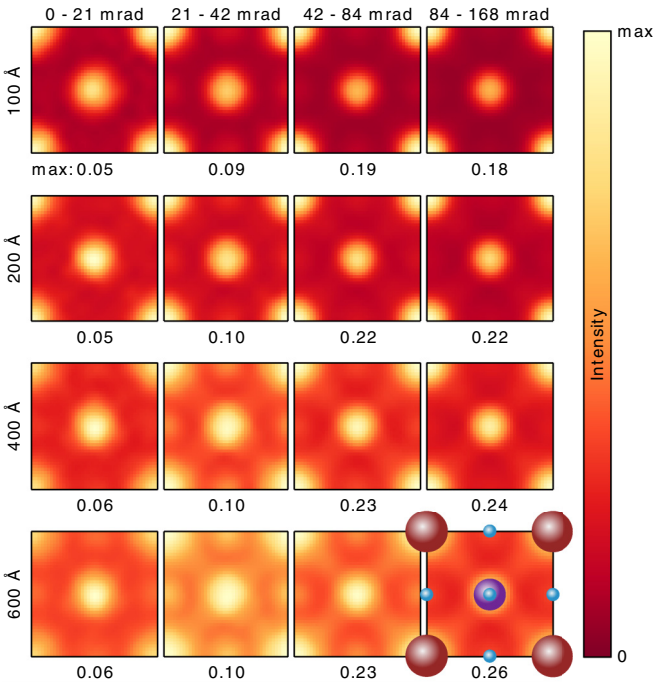

FIG. 3. (Color online) Maps as in Fig. 2 but now with apertures spanning an annular range of scattering angles.

would be obtained by using an energy filter to select only those electrons having lost energy due to phonon excitations. Plasmonic and electronic excitations are not accounted for. These images are each plotted on their own intensity scale, with the maximum fractional intensity indicated below the image. Figure 3 shows similar images but now the apertures span an annular region of the diffraction plane. This shows in more detail how image formation occurs for different ranges of scattering angle. Localized images are obtained, even for scattering through the smallest range of angles.

While the images in Fig. 2 may appear to be qualitatively similar to those in Fig. 2 of the paper by Egoavil *et al.* [3], they are not directly comparable. In that work, the raw data have been processed in two ways. Only the second may isolate information on the signal due to excitation of phonons and this is predicated on the zero-loss peak being of a similar shape for all probe positions. That being the case, the signal obtained at a given probe position is a weighted comparison between the phonon sector of the energy-loss spectrum and the average of the same spectra across all probe positions. The weighting varies from one probe position to the next, making even qualitative comparison with simulations such as those done here problematic. This issue would be remedied by direct subtraction of the zero-loss peak at each probe position.

Figure 4 shows intensity profiles calculated for line scans across the strontium and titanium/oxygen columns, for a specimen thickness of 200 Å and for the same range of detector apertures as in Fig. 3. All intensity profiles have been rescaled so that their maximum value is 1. It was noted earlier that the images in Fig. 3 exhibit localization around the atomic columns. Looking at this localization more closely in Fig. 4, we note the interesting fact that the localization of the STEM image is very similar across the four detectors. In this case the localization of thermal scattering at low angles is not

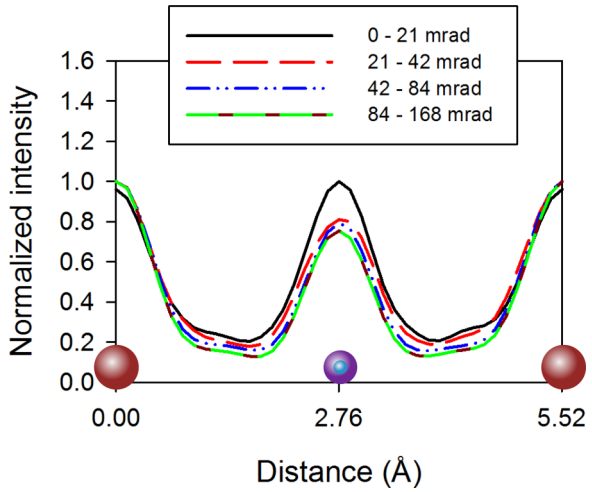

FIG. 4. (Color online) Intensity profiles taken across strontium and titanium/oxygen columns for the data in Fig. 3 corresponding to a specimen thickness of 200 Å. Each profile has the maximum value normalized to unity. Large (brown) circles indicate columns of strontium atoms, medium (brown) circles indicate the presence of titanium atoms in a column, and small (blue) circles indicate the presence of oxygen atoms.

very different from that at large angles. The large momentum transfer associated with scattering into the 82–168 mrad detector (HAADF) does not seem to be a prerequisite for localized imaging using inelastic scattered electrons that have excited a phonon.

VII. CONCLUSION

We have reworked the quantum excitation of phonons (QEP) model [7] in a way which establishes that the contribution from inelastic phonon excitation and deexcitation is included and can be isolated so as to model electron energy-loss spectroscopy in the phonon sector. The energy losses that must necessarily occur during phonon excitation are identified within the theoretical framework presented and furthermore this model has the ability to separate the scattered intensity into elastically and thermally scattered components. We have demonstrated that the effects of phonon excitations of the scattering target are indeed included in the predicted intensity by formally calculating the thermally scattered intensity in both the QEP model and in the transition potential formulation (for the case of a single oscillating atom). Thermal statistics have been included by summing over initial target states drawn from a thermal statistical ensemble.

Simulations of the thermally scattered intensity have been performed for the case of a convergent probe scanned across a specimen while the flux of thermally scattered electrons into an aperture is recorded. These simulations confirm that atomic resolution imaging using energy-loss electrons in the phonon-loss sector is possible.

ACKNOWLEDGMENTS

We would like to thank J. Verbeeck and N. Gauquelin for stimulating discussions. N.R.L. was supported by the Japan Society for the Promotion of Science (JSPS) for this work. This research was supported under the Australian Research Council's Discovery Projects funding scheme (Projects No. DP110102228 and No. DP140102538).

APPENDIX A: DERIVATION OF THE QUANTUM EXCITATION OF PHONONS MODEL

The time-independent Schrödinger equation for the fast electron and target constituents is

$$H(\mathbf{r},\boldsymbol{\tau}_\mathrm{n},\boldsymbol{\tau}_\mathrm{e})\Psi(\mathbf{r},\boldsymbol{\tau}_\mathrm{n},\boldsymbol{\tau}_\mathrm{e}) = E\Psi(\mathbf{r},\boldsymbol{\tau}_\mathrm{n},\boldsymbol{\tau}_\mathrm{e}). \tag{A1}$$

Substituting the factorization of Eq. (8) and writing out the Hamiltonian in full we have

$$[T(\mathbf{r}) + H'(\mathbf{r},\boldsymbol{\tau}_\mathrm{n},\boldsymbol{\tau}_\mathrm{e}) + T_\mathrm{n}(\boldsymbol{\tau}_\mathrm{n}) + T_\mathrm{e}(\boldsymbol{\tau}_\mathrm{e}) + H'_\mathrm{c}(\boldsymbol{\tau}_\mathrm{n},\boldsymbol{\tau}_\mathrm{e})] \times a_0(\boldsymbol{\tau}_\mathrm{n})b(\boldsymbol{\tau}_\mathrm{e},\boldsymbol{\tau}_\mathrm{n})\phi(\mathbf{r},\boldsymbol{\tau}_\mathrm{n}) = Ea_0(\boldsymbol{\tau}_\mathrm{n})b(\boldsymbol{\tau}_\mathrm{e},\boldsymbol{\tau}_\mathrm{n})\phi(\mathbf{r},\boldsymbol{\tau}_\mathrm{n}), \tag{A2}$$

where $T(\mathbf{r})$ is the kinetic energy operator for the fast electron, $H'(\mathbf{r},\boldsymbol{\tau}_\mathrm{n},\boldsymbol{\tau}_\mathrm{e})$ is the interaction potential between the fast electron and the target particles, $T_\mathrm{n}(\boldsymbol{\tau}_\mathrm{n})$ is the kinetic energy operator for the nuclei, $T_\mathrm{e}(\boldsymbol{\tau}_\mathrm{e})$ is the kinetic energy operator for the target electrons, and $H'_\mathrm{c}(\boldsymbol{\tau}_\mathrm{n},\boldsymbol{\tau}_\mathrm{e})$ is the interaction Hamiltonian for the target.

Multiplying Eq. (A2) on the left by $b^*(\boldsymbol{\tau}_\mathrm{e},\boldsymbol{\tau}_\mathrm{n})$ and integrating over the electronic coordinates leads to

$$[T(\mathbf{r}) + \widetilde{H}'(\mathbf{r},\boldsymbol{\tau}_\mathrm{n}) + T_\mathrm{n}(\boldsymbol{\tau}_\mathrm{n}) + K_\mathrm{e} + \widetilde{H}'_\mathrm{c}(\boldsymbol{\tau}_\mathrm{n})]a_0(\boldsymbol{\tau}_\mathrm{n})\phi(\mathbf{r},\boldsymbol{\tau}_\mathrm{n}) = Ea_0(\boldsymbol{\tau}_\mathrm{n})\phi(\mathbf{r},\boldsymbol{\tau}_\mathrm{n}), \tag{A3}$$

where K_e is the total kinetic energy of the target electrons.

Gathering terms and explicitly writing out the term containing $T_\mathrm{n}(\boldsymbol{\tau}_\mathrm{n})$ we obtain

$$[T(\mathbf{r}) + \widetilde{H}'(\mathbf{r},\boldsymbol{\tau}_\mathrm{n})]a_0(\boldsymbol{\tau}_\mathrm{n})\phi(\mathbf{r},\boldsymbol{\tau}_\mathrm{n}) - \sum_j \frac{\hbar^2}{2M_j}\nabla^2_{\boldsymbol{\tau}_\mathrm{n}^j}[a_0(\boldsymbol{\tau}_\mathrm{n})\phi(\mathbf{r},\boldsymbol{\tau}_\mathrm{n})] + \widetilde{H}'_\mathrm{c}(\boldsymbol{\tau}_\mathrm{n})a_0(\boldsymbol{\tau}_\mathrm{n})\phi(\mathbf{r},\boldsymbol{\tau}_\mathrm{n}) = (E - K_\mathrm{e})a_0(\boldsymbol{\tau}_\mathrm{n})\phi(\mathbf{r},\boldsymbol{\tau}_\mathrm{n}). \tag{A4}$$

Using the product rule for Laplacians we have

$$[T(\mathbf{r}) + \widetilde{H}'(\mathbf{r},\boldsymbol{\tau}_\mathrm{n})]a_0(\boldsymbol{\tau}_\mathrm{n})\phi(\mathbf{r},\boldsymbol{\tau}_\mathrm{n}) - \sum_j \frac{\hbar^2}{2M_j}\{a_0(\boldsymbol{\tau}_\mathrm{n})\nabla^2_{\boldsymbol{\tau}_\mathrm{n}^j} + 2\nabla_{\boldsymbol{\tau}_\mathrm{n}^j}a_0(\boldsymbol{\tau}_\mathrm{n})\cdot\nabla_{\boldsymbol{\tau}_\mathrm{n}^j}\}\phi(\mathbf{r},\boldsymbol{\tau}_\mathrm{n})$$
$$- \sum_j \frac{\hbar^2}{2M_j}\phi(\mathbf{r},\boldsymbol{\tau}_\mathrm{n})\nabla^2_{\boldsymbol{\tau}_\mathrm{n}^j}a_0(\boldsymbol{\tau}_\mathrm{n}) + \widetilde{H}'_\mathrm{c}(\boldsymbol{\tau}_\mathrm{n})a_0(\boldsymbol{\tau}_\mathrm{n})\phi(\mathbf{r},\boldsymbol{\tau}_\mathrm{n}) = (E - K_\mathrm{e})a_0(\boldsymbol{\tau}_\mathrm{n})\phi(\mathbf{r},\boldsymbol{\tau}_\mathrm{n}). \tag{A5}$$

Divide through by $a_0(\boldsymbol{\tau}_\mathrm{n})\phi(\mathbf{r},\boldsymbol{\tau}_\mathrm{n})$:

$$\frac{1}{\phi(\mathbf{r},\boldsymbol{\tau}_\mathrm{n})}[T(\mathbf{r})+\widetilde{H}'(\mathbf{r},\boldsymbol{\tau}_\mathrm{n})]\phi(\mathbf{r},\boldsymbol{\tau}_\mathrm{n})-\frac{1}{\phi(\mathbf{r},\boldsymbol{\tau}_\mathrm{n})}\sum_j\frac{\hbar^2}{2M_j}\left\{\nabla^2_{\boldsymbol{\tau}_\mathrm{n}^j}+\frac{2}{a_0(\boldsymbol{\tau}_\mathrm{n})}\nabla_{\boldsymbol{\tau}_\mathrm{n}^j}a_0(\boldsymbol{\tau}_\mathrm{n})\cdot\nabla_{\boldsymbol{\tau}_\mathrm{n}^j}\right\}\phi(\mathbf{r},\boldsymbol{\tau}_\mathrm{n})$$
$$-\sum_j\frac{\hbar^2}{2M_j}\frac{1}{a_0(\boldsymbol{\tau}_\mathrm{n})}\nabla^2_{\boldsymbol{\tau}_\mathrm{n}^j}a_0(\boldsymbol{\tau}_\mathrm{n})+\widetilde{H}'_\mathrm{c}(\boldsymbol{\tau}_\mathrm{n})=E-K_\mathrm{e}. \tag{A6}$$

Note that the terms before the equals sign on the second line depend only on $\boldsymbol{\tau}_\mathrm{n}$. In fact the sum of these terms is equal to $\epsilon_0^{(\mathrm{n})}$, the initial energy of the nuclear subsystem. Thus we get two separate equations:

$$\frac{1}{\phi(\mathbf{r},\boldsymbol{\tau}_\mathrm{n})}[T(\mathbf{r})+\widetilde{H}'(\mathbf{r},\boldsymbol{\tau}_\mathrm{n})]\phi(\mathbf{r},\boldsymbol{\tau}_\mathrm{n})-\frac{1}{\phi(\mathbf{r},\boldsymbol{\tau}_\mathrm{n})}\sum_j\frac{\hbar^2}{2M_j}\left\{\nabla^2_{\boldsymbol{\tau}_\mathrm{n}^j}+\frac{2}{a_0(\boldsymbol{\tau}_\mathrm{n})}\nabla_{\boldsymbol{\tau}_\mathrm{n}^j}a_0(\boldsymbol{\tau}_\mathrm{n})\cdot\nabla_{\boldsymbol{\tau}_\mathrm{n}^j}\right\}\phi(\mathbf{r},\boldsymbol{\tau}_\mathrm{n})=E-K_\mathrm{e}-\epsilon_0^{(\mathrm{n})}, \tag{A7}$$

$$-\sum_i\frac{\hbar^2}{2M_j}\nabla^2_{\boldsymbol{\tau}_\mathrm{n}^j}a_0(\boldsymbol{\tau}_\mathrm{n})+\widetilde{H}'_\mathrm{c}(\boldsymbol{\tau}_\mathrm{n})a_0(\boldsymbol{\tau}_\mathrm{n})=\epsilon_0^{(\mathrm{n})}a_0(\boldsymbol{\tau}_\mathrm{n}). \tag{A8}$$

Noting that the total energy of the system can be decomposed as $E=E_0+\epsilon_0^{(\mathrm{n})}+K_e$, we can rewrite Eq. (A7) as

$$\left[-\frac{\hbar^2}{2m_\mathrm{e}}\nabla^2_\mathbf{r}+\widetilde{H}'(\mathbf{r},\boldsymbol{\tau}_\mathrm{n})-\sum_j\frac{\hbar^2}{2M_j}\left\{\nabla^2_{\boldsymbol{\tau}_\mathrm{n}^j}+\frac{2}{a_0(\boldsymbol{\tau}_\mathrm{n})}\nabla_{\boldsymbol{\tau}_\mathrm{n}^j}a_0(\boldsymbol{\tau}_\mathrm{n})\cdot\nabla_{\boldsymbol{\tau}_\mathrm{n}^j}\right\}\right]\phi(\mathbf{r},\boldsymbol{\tau}_\mathrm{n})=E_0\phi(\mathbf{r},\boldsymbol{\tau}_\mathrm{n}). \tag{A9}$$

APPENDIX B: TRANSITION POTENTIALS FOR A HARMONIC OSCILLATOR

The transition potential $H_{m0}(\mathbf{r})$ is given by [8–10]

$$H_{m0}(\mathbf{r})=\int\xi^*_m(\boldsymbol{\tau}_\mathrm{n},\boldsymbol{\tau}_\mathrm{e})H'(\mathbf{r},\boldsymbol{\tau}_\mathrm{n},\boldsymbol{\tau}_\mathrm{e})\xi_0(\boldsymbol{\tau}_\mathrm{n},\boldsymbol{\tau}_\mathrm{e})\,d\boldsymbol{\tau}_\mathrm{n}\,d\boldsymbol{\tau}_\mathrm{e}, \tag{B1}$$

where $\xi_0(\boldsymbol{\tau}_\mathrm{n},\boldsymbol{\tau}_\mathrm{e})$ and $\xi_m(\boldsymbol{\tau}_\mathrm{n},\boldsymbol{\tau}_\mathrm{e})$ are the initial and final states of the oscillating atom. The interaction Hamiltonian $H'(\mathbf{r},\boldsymbol{\tau}_\mathrm{n},\boldsymbol{\tau}_\mathrm{e})$ is given by

$$H'(\mathbf{r},\boldsymbol{\tau}_\mathrm{n},\boldsymbol{\tau}_\mathrm{e})=\frac{-Ze^2}{4\pi\epsilon_0|\mathbf{r}-\boldsymbol{\tau}_\mathrm{n}|}+\sum_{i=1}^{Z}\frac{e^2}{4\pi\epsilon_0|\mathbf{r}-\boldsymbol{\tau}_\mathrm{e}^i|}, \tag{B2}$$

where Z is the atomic number of the atom, ϵ_0 is the vacuum permittivity, $\boldsymbol{\tau}_\mathrm{n}$ is the position of the nucleus, and $\boldsymbol{\tau}_\mathrm{e}^i$ is the position of the ith atomic electron.

We make the approximation that the electronic motion is as for a stationary atom centered at the parametric position $\boldsymbol{\tau}_\mathrm{n}$ of that atom. We also make a ground state approximation for the atomic electrons. We can thus express the target state as

$$\xi_m(\boldsymbol{\tau}_\mathrm{n},\boldsymbol{\tau}_\mathrm{e})=a_m(\boldsymbol{\tau}_\mathrm{n})b(\boldsymbol{\tau}_\mathrm{e}), \tag{B3}$$

where $a_m(\boldsymbol{\tau}_\mathrm{n})$ is the final state of the harmonic oscillator and $b(\boldsymbol{\tau}_\mathrm{e})$ is the ground state wave function of the atomic electrons, with the electronic coordinates $\boldsymbol{\tau}_\mathrm{e}$ defined relative to the nuclear coordinate $\boldsymbol{\tau}_\mathrm{n}$.

It will prove easier to work in reciprocal space; thus,

$$H_{m0}(\mathbf{q})=\int H_{m0}(\mathbf{r})e^{-2\pi i\mathbf{q}\cdot\mathbf{r}}\,d\mathbf{r}. \tag{B4}$$

With use of the standard identity

$$\int\frac{1}{|\mathbf{r}-\mathbf{r}'|}e^{-2\pi i\mathbf{q}\cdot\mathbf{r}}\,d\mathbf{r}=\frac{1}{\pi|\mathbf{q}|^2}e^{-2\pi i\mathbf{q}\cdot\mathbf{r}'}, \tag{B5}$$

we find that

$$H_{m0}(\mathbf{q})=\frac{-Ze^2}{4\pi^2\epsilon_0|\mathbf{q}|^2}\int a^*_m(\boldsymbol{\tau}_\mathrm{n})b^*(\boldsymbol{\tau}_\mathrm{e})e^{-2\pi i\mathbf{q}\cdot\boldsymbol{\tau}_\mathrm{n}}$$
$$\times a_0(\boldsymbol{\tau}_\mathrm{n})b(\boldsymbol{\tau}_\mathrm{e})\,d\boldsymbol{\tau}_\mathrm{n}\,d\boldsymbol{\tau}_\mathrm{e}$$
$$+\sum_{i=1}^{Z}\frac{e^2}{4\pi^2\epsilon_0|\mathbf{q}|^2}\int a^*_m(\boldsymbol{\tau}_\mathrm{n})b^*(\boldsymbol{\tau}_\mathrm{e})e^{-2\pi i\mathbf{q}\cdot(\boldsymbol{\tau}_\mathrm{e}^i+\boldsymbol{\tau}_\mathrm{n})}$$
$$\times a_0(\boldsymbol{\tau}_\mathrm{n})b(\boldsymbol{\tau}_\mathrm{e})\,d\boldsymbol{\tau}_\mathrm{n}\,d\boldsymbol{\tau}_\mathrm{e}. \tag{B6}$$

Performing the integrals over electronic coordinates and gathering terms we have

$$H_{m0}(\mathbf{q})=\frac{-e^2}{4\pi^2\epsilon_0|\mathbf{q}|^2}[Z-f_\mathrm{x}(\mathbf{q})]$$
$$\times\int a^*_m(\boldsymbol{\tau}_\mathrm{n})a_0(\boldsymbol{\tau}_\mathrm{n})e^{-2\pi i\mathbf{q}\cdot\boldsymbol{\tau}_\mathrm{n}}\,d\boldsymbol{\tau}_\mathrm{n}, \tag{B7}$$

where $f_\mathrm{x}(\mathbf{q})$ is the x-ray scattering factor given by

$$f_\mathrm{x}(\mathbf{q})=\sum_{i=1}^{Z}\int|b(\boldsymbol{\tau}_\mathrm{e})|^2e^{-2\pi i\mathbf{q}\cdot\boldsymbol{\tau}_\mathrm{e}^i}\,d\boldsymbol{\tau}_\mathrm{e}. \tag{B8}$$

Making use of the Mott-Bethe formula

$$f_\mathrm{e}(\mathbf{q})=\frac{e}{4\pi^2\epsilon_0}\frac{Z-f_\mathrm{x}(\mathbf{q})}{|\mathbf{q}|^2}, \tag{B9}$$

where $f_\mathrm{e}(\mathbf{q})$ is the electron scattering factor, we find that

$$H_{m0}(\mathbf{q})=-ef_\mathrm{e}(\mathbf{q})\int a^*_m(\boldsymbol{\tau}_\mathrm{n})a_0(\boldsymbol{\tau}_\mathrm{n})e^{-2\pi i\mathbf{q}\cdot\boldsymbol{\tau}_\mathrm{n}}\,d\boldsymbol{\tau}_\mathrm{n}. \tag{B10}$$

APPENDIX C: GENERAL ILLUMINATION

1. Transition potential formulation

To treat the case of general illumination, we return to Eq. (25) and write out the convolution explicitly:

$$\begin{aligned}\psi_m(\mathbf{q}_\perp) &= i\sigma e\left[f_e(\mathbf{q}_\perp)\int a_m^*(\boldsymbol{\tau}_n)a_0(\boldsymbol{\tau}_n)e^{-2\pi i\mathbf{q}_\perp\cdot\boldsymbol{\tau}_n}\,d\boldsymbol{\tau}_n\right]\otimes\psi_0(\mathbf{q}_\perp)\\ &= i\sigma e\int\psi_0(\mathbf{q}'_\perp)f_e(\mathbf{q}_\perp-\mathbf{q}'_\perp)\int a_m^*(\boldsymbol{\tau}_n)a_0(\boldsymbol{\tau}_n)e^{-2\pi i(\mathbf{q}_\perp-\mathbf{q}'_\perp)\cdot\boldsymbol{\tau}_n}\,d\boldsymbol{\tau}_n\,d\mathbf{q}'_\perp.\end{aligned}\tag{C1}$$

The corresponding intensity is

$$\begin{aligned}I_m(\mathbf{q}_\perp) &= |\psi_m(\mathbf{q}_\perp)|^2\\ &= \sigma^2e^2\iint\psi_0^*(\mathbf{q}''_\perp)\psi_0(\mathbf{q}'_\perp)f_e(\mathbf{q}_\perp-\mathbf{q}''_\perp)f_e(\mathbf{q}_\perp-\mathbf{q}'_\perp)\iint a_m(\boldsymbol{\tau}'_n)a_m^*(\boldsymbol{\tau}_n)a_0^*(\boldsymbol{\tau}'_n)a_0(\boldsymbol{\tau}_n)\\ &\quad\times e^{2\pi i(\mathbf{q}_\perp-\mathbf{q}''_\perp)\cdot\boldsymbol{\tau}'_n}e^{-2\pi i(\mathbf{q}_\perp-\mathbf{q}'_\perp)\cdot\boldsymbol{\tau}_n}\,d\boldsymbol{\tau}_n\,d\boldsymbol{\tau}'_n\,d\mathbf{q}'_\perp\,d\mathbf{q}''_\perp.\end{aligned}\tag{C2}$$

The thermally scattered intensity is given by

$$\begin{aligned}I_{th}(\mathbf{q}_\perp) &= \sum_{m\neq0}I_m(\mathbf{q}_\perp)\\ &= \left[\sum_m I_m(\mathbf{q}_\perp)\right]-I_0(\mathbf{q}_\perp)\\ &= \sigma^2e^2\iint\psi_0^*(\mathbf{q}''_\perp)\psi_0(\mathbf{q}'_\perp)f_e(\mathbf{q}_\perp-\mathbf{q}''_\perp)f_e(\mathbf{q}_\perp-\mathbf{q}'_\perp)\mathcal{A}(\mathbf{q}_\perp,\mathbf{q}'_\perp,\mathbf{q}''_\perp)\,d\mathbf{q}'_\perp\,d\mathbf{q}''_\perp,\end{aligned}\tag{C3}$$

where

$$\mathcal{A}(\mathbf{q}_\perp,\mathbf{q}'_\perp,\mathbf{q}''_\perp)=\int|a_0(\boldsymbol{\tau}_n)|^2e^{-2\pi i(\mathbf{q}''_\perp-\mathbf{q}'_\perp)\cdot\boldsymbol{\tau}_n}\,d\boldsymbol{\tau}_n-\left[\int|a_0(\boldsymbol{\tau}_n)|^2e^{2\pi i(\mathbf{q}_\perp-\mathbf{q}''_\perp)\cdot\boldsymbol{\tau}_n}\,d\boldsymbol{\tau}_n\int|a_0(\boldsymbol{\tau}_n)|^2e^{-2\pi i(\mathbf{q}_\perp-\mathbf{q}'_\perp)\cdot\boldsymbol{\tau}_n}\,d\boldsymbol{\tau}_n\right].\tag{C4}$$

In Eq. (C3) above we have used the completeness identity $\sum_m a_m(\boldsymbol{\tau}'_n)a_m^*(\boldsymbol{\tau}_n)=\delta(\boldsymbol{\tau}'_n-\boldsymbol{\tau}_n)$.

2. QEP model

In a similar manner to the previous section, to treat the case of general illumination within the QEP model we return to Eq. (31) and explicitly write out the convolution:

$$\begin{aligned}\phi(\mathbf{q}_\perp,\boldsymbol{\tau}_n) &= i\sigma e[f_e(\mathbf{q}_\perp)e^{-2\pi i\mathbf{q}_\perp\cdot\boldsymbol{\tau}_n}]\otimes\psi_0(\mathbf{q}_\perp)\\ &= i\sigma e\int\psi_0(\mathbf{q}'_\perp)f_e(\mathbf{q}_\perp-\mathbf{q}'_\perp)e^{-2\pi i(\mathbf{q}_\perp-\mathbf{q}'_\perp)\cdot\boldsymbol{\tau}_n}\,d\mathbf{q}'_\perp.\end{aligned}\tag{C5}$$

The corresponding intensity is

$$|\phi(\mathbf{q}_\perp,\boldsymbol{\tau}_n)|^2=\sigma^2e^2\iint\psi_0^*(\mathbf{q}''_\perp)\psi_0(\mathbf{q}'_\perp)f_e(\mathbf{q}_\perp-\mathbf{q}''_\perp)f_e(\mathbf{q}_\perp-\mathbf{q}'_\perp)e^{-2\pi i(\mathbf{q}''_\perp-\mathbf{q}'_\perp)\cdot\boldsymbol{\tau}_n}\,d\mathbf{q}'_\perp\,d\mathbf{q}''_\perp.\tag{C6}$$

The thermally scattered intensity is given by [see Eq. (19)]

$$\begin{aligned}I_{th}(\mathbf{r}) &= \int|a_0(\boldsymbol{\tau}_n)|^2|\phi(\mathbf{r},\boldsymbol{\tau}_n)|^2\,d\boldsymbol{\tau}_n-\left|\int|a_0(\boldsymbol{\tau}_n)|^2\phi(\mathbf{r},\boldsymbol{\tau}_n)\,d\boldsymbol{\tau}_n\right|^2\\ &= \sigma^2e^2\iint\psi_0^*(\mathbf{q}''_\perp)\psi_0(\mathbf{q}'_\perp)f_e(\mathbf{q}_\perp-\mathbf{q}''_\perp)f_e(\mathbf{q}_\perp-\mathbf{q}'_\perp)\mathcal{A}(\mathbf{q}_\perp,\mathbf{q}'_\perp,\mathbf{q}''_\perp)\,d\mathbf{q}'_\perp\,d\mathbf{q}''_\perp,\end{aligned}\tag{C7}$$

where $\mathcal{A}(\mathbf{q}_\perp,\mathbf{q}'_\perp,\mathbf{q}''_\perp)$ is given in Eq. (C4). This result is identical to Eq. (C3) obtained within the transition potential formulation.

APPENDIX D: STATISTICS

Taking a thermal average over possible initial states, the probability distribution for motion in a single direction of a single harmonic oscillator is [see Eq. (38)]

$$P(x) = \frac{1}{\mathcal{Z}} \sum_n e^{-E_n\beta} |g_n(x)|^2, \tag{D1}$$

where $E_n = \hbar\omega(n + \frac{1}{2})$ is the energy of the nth thermal state, $\beta = 1/k_B T$, k_B is the Boltzmann constant, T is the temperature, $g_n(x)$ is the nth Hermite function, and $\mathcal{Z}$ is the partition function, given by

$$\mathcal{Z} = \sum_n e^{-E_n\beta} = \frac{e^{-\hbar\omega\beta/2}}{1 - e^{-\hbar\omega\beta}}. \tag{D2}$$

Letting $u = e^{-\hbar\omega\beta}$ we have

$$P(x) = (1 - u) \sum_n u^n |g_n(x)|^2. \tag{D3}$$

We make use of the Hermite function identity

$$\sqrt{\frac{\hbar}{M\omega}} \sum_{n=0}^{\infty} u^n |g_n(x)|^2 = \frac{1}{\sqrt{\pi(1-u^2)}} \exp\left(-\frac{1-u}{1+u}\frac{M\omega}{\hbar}x^2\right). \tag{D4}$$

The probability distribution can then be written as

$$\begin{aligned} P(x) &= \sqrt{\frac{M\omega}{\hbar}}(1-u)\frac{1}{\sqrt{\pi(1-u^2)}} \exp\left(-\frac{1-u}{1+u}\frac{M\omega}{\hbar}x^2\right) \\ &= \sqrt{\frac{M\omega}{\hbar}\frac{1-u}{\pi(1+u)}} \exp\left(-\frac{1-u}{1+u}\frac{M\omega}{\hbar}x^2\right) \\ &\equiv \frac{1}{\sqrt{2\pi\sigma^2}} e^{-x^2/2\sigma^2}, \end{aligned} \tag{D5}$$

where we have defined

$$\begin{aligned} \sigma^2 &\equiv \frac{\hbar}{2M\omega}\frac{1+u}{1-u} \\ &= \frac{\hbar}{2M\omega} \coth\left(\frac{\hbar\omega\beta}{2}\right). \end{aligned} \tag{D6}$$

[1] C. Dwyer, Phys. Rev. B **89**, 054103 (2014).
[2] P. Rez, Microsc. Microanal. **20**, 671 (2014).
[3] R. Egoavil, N. Gauquelin, G. Martinez, S. Van Aert, G. Van Tendeloo, and J. Verbeeck, Ultramicroscopy **147**, 1 (2014).
[4] R. Brydson, Nature (London) **514**, 177 (2014).
[5] J. Spence and J. Zuo, Ultramicroscopy **69**, 185 (1997).
[6] O. L. Krivanek, T. C. Lovejoy, N. Dellby, T. Aoki, R. W. Carpenter, P. Rez., E. Soignard, J. Zhu, P. E. Batson, M. J. Lagos, R. F. Egerton, and P. A. Crozier, Nature (London) **514**, 209 (2014).
[7] B. D. Forbes, A. V. Martin, S. D. Findlay, A. J. D'Alfonso, and L. J. Allen, Phys. Rev. B **82**, 104103 (2010).
[8] W. Coene and D. Van Dyck, Ultramicroscopy **33**, 261 (1990).
[9] C. Dwyer, Ultramicroscopy **104**, 141 (2005).
[10] N. R. Lugg, B. Freitag, S. D. Findlay, and L. J. Allen, Ultramicroscopy **110**, 981 (2010).
[11] H. Yoshioka, J. Phys. Soc. Jpn. **12**, 618 (1957).
[12] A. Weickenmeier and H. Kohl, Acta Crystallogr., Sect. A **54**, 283 (1998).
[13] A. V. Martin, S. D. Findlay, and L. J. Allen, Phys. Rev. B **80**, 024308 (2009).
[14] M. Born and R. Oppenheimer, Ann. Phys. (Leipzig) **389**, 457 (1927).